Scientia Iranica A (2018) 25(3), 1105–1121

SCIENTIA IRANICA

Sharif University of Technology
**Scientia Iranica**
*Transactions A: Civil Engineering*
http://scientiairanica.sharif.edu

# A node-based smoothed finite-element method for stability analysis of dual square tunnels in cohesive-frictional soils

**T. Vo-Minh[a,b,*], A. Chau-Ngoc[a], T. Nguyen-Minh[a], and H. Nguyen-Chanh[b]**

a. *Department of Civil Engineering, Ho Chi Minh City University of Technology, HCMUT, Vietnam.*
b. *Department of Civil Engineering, HCMC University of Technology, Hutech, Vietnam.*

Received 24 September 2016; received in revised form 5 November 2016; accepted 28 January 2017

**KEYWORDS**
Limit analysis;
Dual square tunnels;
Stability;
NS-FEM;
SOCP.

**Abstract.** This paper presents an upper-bound limit analysis procedure using the node-based Smoothed Finite-Element Method (NS-FEM) and Second-Order Cone Programming (SOCP) to evaluate the stability of dual square tunnels in cohesive-frictional soils subjected to surcharge loading. The displacement field of the tunnel problems is approximated using NS-FEM triangular elements (NS-FEM-T3). Next, commercial software Mosek is employed to deal with optimization problems, which are formulated as second-order cone. Collapse loads and failure mechanisms of dual square tunnels are performed by solving the optimization problems with a series of size-to-depth ratios and soil properties. For dual square tunnels, the distance between centers of two parallel tunnels is the major parameter used to determine the stability. In this study, surcharge loading is applied to the ground surface, and drained conditions are considered. Numerical results are verified with those available to demonstrate the accuracy of the proposed method.



## 1. Introduction

In recent years, underground systems have become essential for the rapid development of many major cities. In fact, such underground infrastructures as underground railway and gas pipeline have become increasingly popular in many metropolises to meet the demands of citizens. During the construction of such underground networks, the depth of tunnels needs to be investigated carefully, because this plays an important role in constructing process and may help to reduce the cost of constructions. Moreover, in order to construct safe and stable tunnel systems in highly populous cities, engineers need to determine the loading limit and failure mechanism of tunnels subjected to surcharge loading distributed on the ground.

In cohesive-frictional soils, limit equilibrium methods are widely used to determine the face stability of tunnel. By using 2D logarithmic spiral failure mechanism, Muragana et al. [1] calculated the limit support pressure of the tunnel face. Based on a limit equilibrium analytical approach, Krause [2] determined the limit support pressure for tunnel face by assuming different failure zone shapes. Later, Horn [3] proposed 3D failure mechanism to investigate the limit support pressure of the tunnel face. The other analytical approaches were limit analysis methods based on the upper- and lower-bound theorems. In 1980, Davis et al. [4] proposed a theoretical solution for single

*. *Corresponding author. Tel.: +84-903924005*
*E-mail addresses: vm.thien@hutech.edu.vn (T. Vo-Minh); cnan@hcmut.edu.vn (A. Chau-Ngoc); nmtam@hcmut.edu.vn (T. Nguyen-Minh); nchoangoxf@gmail.com (H. Nguyen-Chanh)*

doi: 10.24200/sci.2018.20193

circular tunnel in cohesive material under undrained condition using both upper-bound and lower-bound limit analyses. In the study of Mühlhaus [5], lower bound approach was applied to evaluate the stability of tunnels subject to uniform internal pressure. Leca and Dormieux [6] used the upper-bound and lower-bound limit analyses to determine the limit support pressure in frictional material by assuming the failure zone in front of the tunnel face consisted of a series of conical bodies. Recently, Chengping Zhang et al. [7] proposed a new 3D failure mechanism using the kinematic approach of limit analysis theory to determine the limit support pressure of the tunnel face.

On the other hand, experimental tests can be used to study tunnel face stability problems and failure mechanism. A series of centrifuge model tests of tunnels in dry sand were described by Atkinson and Pott [8]. Atkinson and Cairncross [9] investigated the failure mechanism of circular tunnels when considering soil behaviour as a uniform Mohr-Coulomb material. In the study of Cairncross [10], experiment approach was used to determine the deformation around a circular tunnel in stiff clay. In 1979, Seneviratne [11] investigated the influence of pore-pressure on the stability of circular tunnels in soft clay. Mair [12] also conducted some centrifugal model tests to estimate the stability of circular tunnels in soft clay for plane strain. In 1994, Chambon and Corté [13] conducted a series of centrifuge tests to evaluate the tunnel face stability in sand. Recently, Kirsch [14] and Idinger et al. [15] performed small-scale tunnel model in geotechnical centrifuge to investigate the face stability of shallow tunnel in dry sand. Ground deformation and failure mechanism were measured by digital image correlation. However, most of the theoretical studies were only focused on stability of a single tunnel. There is scarcity of evidence in literature which suggests determining the stability of twin tunnels. To investigate the stability of two parallel tunnels, a series of centrifuge model tests for clays were conducted by Wu and Lee [16], and their studies were aimed to formulate ground movements and failure mechanisms of soils surrounding two tunnels. Chahade and Shahrour [17] used Plaxis software to simulate the construction procedure of twin tunnels with various distances between their centers, and then considered its influence on tunnels stability. The upper-bound limit analysis was also applied in Osman's study [18] to evaluate the stability of twin circular tunnels for large-scale engineering problems. In addition, ABAQUS was used in the research of Mirhabibi and Soroush [19] to estimate the influence of construction load on the movement of soil surrounding two tunnels.

In recent decades, the standard Finite-Element Method (FEM) has been rapidly developing to solve complicated engineering problems. A finite-element procedure for linear analysis was first given by Sloan and Assadi [20] to evaluate the undrained stability of a square tunnel in a soil whose shear strength increases linearly with depth. Lyamin and Sloan [21], Lyamin et al. [22], and Yamamoto et al. [23,24] developed FEM-based nonlinear analysis methods to calculate the failure mechanisms of circular and square tunnels in cohesive-frictional soils. In the study of Sahoo and Kumar [25], a procedure using FEM and linear programming was employed to investigate the stability of two circular tunnels in clay. Yamamoto et al. [26,27] proposed an efficient method to assess the stability of dual circular and dual square tunnels in cohesive material; however, the nonlinear optimization procedure required large computational efforts. Recently, Wilson et al. [28,29] investigated the undrained stability of dual circular tunnels and dual square tunnels using FEM and Second-Order Cone Programming (SOCP).

Due to the simplicity, the standard Finite-Element Method using triangular element (FEM-T3) has gained popularity. One of the marked drawbacks to FEM-T3 elements is volumetric locking phenomenon, which often occurs in the nearly incompressible materials. To overcome this, many methods were suggested to reduce integration methods [30], B-bar methods [31], enhanced assumed strain [32-34], average nodal technique [35], and so on. In this study, NS-FEM that is originated from integration methods is used to overcome the challenge of volumetric locking. More precisely, the idea of the nodal integration in a meshfree method using the strain smoothing technique was proposed by Chen and his collaborators [36,37]. Then, Liu and Nguyen-Thoi [38] applied this technique to standard FEM to provide a softening effect so as to improve the solution of FEM, which is called Smoothed Finite-Element Method (S-FEM), including Cell-based Smoothed FEM (CS-FEM) [39], Node-based Smoothed FEM (NS-FEM) [40], Face-based Smoothed FEM (FS-FEM) [41], and Edge-based Smoothed FEM (ES-FEM) [42]. In these S-FEM models, the finite-element mesh is used similarly as in FEM models. However, these S-FEM models evaluate the weak form based on smoothing domains created from the entities of the element mesh, such as cells/elements, or nodes, or faces, or edges. These smoothing domains can be located inside the elements (CS-FEM) or cover parts of adjacent elements (NS-FEM, FS-FEM, and ES-FEM). These smoothing domains are linearly independent and ensure the stability and convergence of the S-FEM models. The theoretical aspect of the S-FEM is clearly presented in [43,44]. Several further developments of S-FEMs for limit and shakedown analysis have been investigated in [45-49].

Nowadays, the Node-based Smoothed Finite-Element Method (NS-FEM) has been employed for upper and lower bound limit problems due to the following advantages: (i) Total number of degrees of freedom significantly decreases, leading to a fast convergence for solutions, (ii) Volumetric locking phenomenon is prevented using NS-FEM method in solving undrained (incompressible) problems, because elements do not have enough necessary degrees of freedom to find solutions with the condition of constant volume, (iii) By using smoothed strains in NS-FEM, the integration is conducted in the edges of smoothed cells; as a results, there is no need to compute the first derivation of shape functions. Studies demonstrate that the NS-FEM performs well in heat transfer analysis [50,51], fracture analysis [52], acoustic problems [53,54], axisymmetric shell structures [55], and static and dynamic analyses [56-58]. Recently, Vo-Minh et al. [59] applied an upper-bound limit analysis using the Node-based Smoothed Finite-Element Method (NS-FEM) and Second-Order Cone Programming (SOCP) to determine the stability of dual circular tunnels in cohesive-frictional soils.

In upper-bound limit analysis, the internal plastic dissipation is minimized to determine the ultimate load bearing capacity of the soils. The Mohr-Coulomb yield criterion can be formed in a Second-Order Cone Programming (SOCP). To solve the resulting conic problems, the MATLAB (version 7.8.0) and the Mosek (version 6.0) [60] are used to present all solutions in this paper. The Mosek optimization toolbox can solve only convex optimization problems, such as linear, quadratic, and conic programming. Large-scale SOCP problems can be solved effectively using primal-dual algorithms based on the interior-point method. This algorithm was proved an effective optimization technique for limit analysis of the soils.

This paper focuses on the stability analysis of dual square tunnels in cohesive-frictional soil subjected to surcharge loading using the Node-based Smoothed Finite-Element Method (NS-FEM) and Second-Order Cone Programming (SOCP). Collapse loads and failure mechanisms of dual square tunnels were performed by solving the optimization problems with a series of size-to-depth ratios and soil properties. We also presented a variety of examples to evaluate the influence of the distance between two tunnels on the stability. To evaluate the accuracy of this suggested procedure, the obtained results are compared with those of Yamamoto et al. [27].

This paper is outlined as follows. In Section 2, the problem definition is described. The brief on the node-based smoothed finite-element method NS-FEM is introduced in Section 3. NS-FEM formulation for plane strain with Mohr-Coulomb yield criterion is presented in Section 4. In Section 5, some numerical examples are performed and discussed to demonstrate the effectiveness of the presented method. Some concluding remarks are made in Section 6.

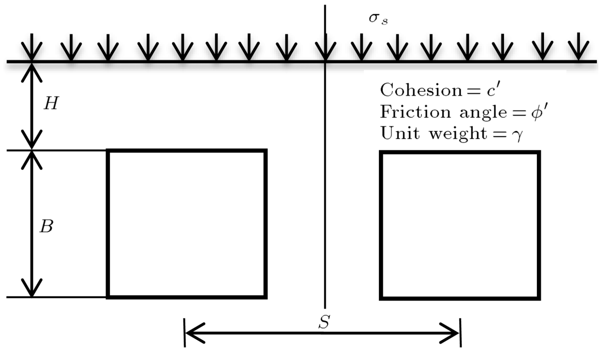


**Figure 1.** Twin square tunnels subjected to surcharge loading.

## 2. Problem definition

The twin square tunnels which are of width, $B$, depth, $H$, and distance between tunnels, $S$, are illustrated as in Figure 1. The ground deformation takes place under plane strain. For cohesive-frictional soil, the soil behavior is described as a uniform Mohr-Coulomb material with value of cohesion, $c'$, friction angle, $\phi'$, and unit weight, $\gamma$. Drained loading conditions are also considered, and surcharge loading is applied to the ground surface. In order to assess the stability of the tunnel, a dimensionless load factor, $\sigma_s/c'$, is defined using a function of $\phi'$, $\gamma B/c'$, $S/B$, and $H/B$, as shown in the following equation:

$$\frac{\sigma_s}{c'} = f\left(\phi', \frac{\gamma B}{c'}, \frac{H}{B}, \frac{S}{B}\right). \tag{1}$$

In order to investigate stability number, $\sigma_s/c'$, the variations in parameters considered are $H/B = 1 - 5$, $\phi' = 00 - 200$, $\gamma B/c' = 0 - 3$, and tunnel spacing $S/B = 1.25 - 12.5$. In the analyzed model, the interface condition between the loading and the soil was smooth.

## 3. Brief on the Node-based Smoothed Finite-Element Method (NS-FEM)

The strain smoothing technique was proposed by Chen et al. [36,37] to stabilize the solution in the nodal integrated meshfree methods. Later, it was introduced into FEM by Liu and his collaborators [38-44] to form S-FEM, such as ES-FEM, CS-FEM, NS-FEM, and so on. The main difference between S-FEM and the standard FEM is the strain field. In standard FEM, the displacement field is assumed, and the strain is calculated from the strain-displacement relation. In S-FEM, a strain smoothing is calculated from the strain in FEM by a smoothed function. In this paper, the formulation of smoothing function using NS-FEM is presented.

In NS-FEM, the integration based on nodes and strain smoothing technique is used. The problem domain, $\Omega$, is divided into $N_n$ smoothing cells, $\Omega^{(k)}$, associated with node $k$, such that $\Omega = \sum_{k=1}^{N_n} \Omega^{(k)}$ and $\Omega^i \cap \Omega^j = \phi$, $i \neq j$, and $N_n$ is the total number of field nodes located in the entire problem domain. Each of triangular elements will be divided into three quadrilateral subdomains, and each quadrilateral subdomain is attached to the nearest field node.

A strain smoothing formulation on cell $\Omega^{(k)}$ is now defined by the following operation:

$$\tilde{\varepsilon}_k = \int_{\Omega^{(k)}} \varepsilon(\mathbf{x})\Phi_k(\mathbf{x})d\Omega = \int_{\Omega^{(k)}} \nabla_s \mathbf{u}(\mathbf{x})\Phi_k(\mathbf{x})d\Omega, \tag{2}$$

where $\Phi_k(\mathbf{x})$ is a smoothing function that satisfies positive criteria which is normalized to unity:

$$\int_{\Omega^{(k)}} \Phi_k(\mathbf{x})d\Omega = 1. \tag{3}$$

Smoothing function, $\Phi_k(x)$, is assumed constant as follows:

$$\Phi_k(\mathbf{x}) = \begin{cases} 1/A^{(k)}, & \mathbf{x} \in \Omega^{(k)} \\ 0, & \mathbf{x} \notin \Omega^{(k)} \end{cases} \tag{4}$$

where $A^{(k)} = \int_{\Omega^{(k)}} d\Omega$ is the area of cell $\Omega^{(k)}$ and the smoothed strain on domain $\Omega^{(k)}$ can be expressed as follows:

$$\tilde{\varepsilon}_k = \frac{1}{A^{(k)}} \int_{\Gamma^{(k)}} \mathbf{u}(\mathbf{x})\mathbf{n}^{(k)}(\mathbf{x})d\Gamma, \tag{5}$$

where $\Gamma^{(k)}$ is the boundary of domain $\Omega^{(k)}$ as shown in Figure 2 and $\mathbf{n}^{(k)}$ is a matrix with components of the outward normal vector on boundary $\Gamma^{(k)}$ given by:

$$\mathbf{n}^{(k)}(\mathbf{x}) = \begin{bmatrix} n_x^{(k)} & 0 \\ 0 & n_y^{(k)} \\ n_y^{(k)} & n_x^{(k)} \end{bmatrix}. \tag{6}$$

The smoothed strain on cell $\Omega^{(k)}$ associated with node $k$ can be calculated by:

$$\tilde{\varepsilon}_k = \sum_{I \in N^{(k)}} \tilde{\mathbf{B}}_I(\mathbf{x}_k)\mathbf{d}_I, \tag{7}$$

where $N^{(k)}$ is the set containing nodes that are directly connected to node $k$, $\mathbf{d}_I$ is the nodal displacement vector, and the smoothed strain gradient matrix, $\tilde{\mathbf{B}}_I(\mathbf{x}_k)$, on domain $\Omega^{(k)}$ can be determined from:

$$\tilde{\mathbf{B}}_I(\mathbf{x}_k) = \begin{bmatrix} \tilde{b}_{Ix}(\mathbf{x}_k) & 0 \\ 0 & \tilde{b}_{Iy}(\mathbf{x}_k) \\ \tilde{b}_{Iy}(\mathbf{x}_k) & \tilde{b}_{Ix}(\mathbf{x}_k) \end{bmatrix}, \tag{8}$$

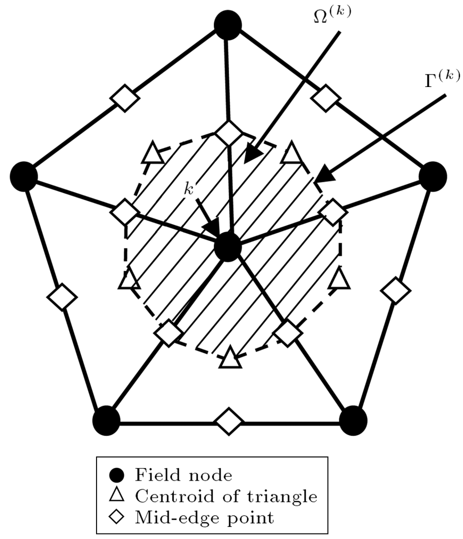


**Figure 2.** Triangular elements and smoothing cells associated with the nodes in the NS-FEM.

where:

$$\tilde{b}_{Ih}(\mathbf{x}_k) = \frac{1}{A^{(k)}} \int_{\Gamma^{(k)}} n_h^{(k)}(\mathbf{x})\mathbf{N}_I(\mathbf{x})d\Gamma, \tag{9}$$

when a linear compatible displacement field along boundary $\Gamma^{(k)}$ is used, one Gauss point is sufficient for line integration along each segment of boundary $\Gamma^{(k)}$ of $\Omega^{(k)}$, and then the above equation can be determined as follows:

$$\tilde{b}_{Ih}(\mathbf{x}_k) = \frac{1}{A^{(k)}} \sum_{i=1}^{M} \mathbf{N}_I(\mathbf{x}_i^{GP}) n_{ih}^{(k)} l_i^{(k)}, (h = x, y), \tag{10}$$

where $M$ is the total number of the boundary segment of $\Gamma_i^{(k)}$, $\mathbf{x}_i^{GP}$ is the Gauss point of the boundary segment of $\Gamma_i^{(k)}$ which has length $l_i^{(k)}$ and outward unit normal $n_{ih}^{(k)}$.

## 4. Upper-bound limit analysis procedure using the Node-based Smoothed Finite-Element Method (NS-FEM)

The soil is assumed to be perfectly plastic, and it obeys the Mohr-Coulomb failure criterion and associated flow rule. The Mohr-Coulomb yield function can be expressed in the form of stress components as follows:

$$\psi(\sigma) = \sqrt{(\sigma_{xx} - \sigma_{yy})^2 + 4\tau_{xy}^2} + (\sigma_{xx} + \sigma_{yy})\sin\phi' - 2c'.\cos\phi'. \tag{11}$$

For an associated flow rule, the direction of the plastic strain rates vector is given by the gradient to the yield function with its magnitude given by plastic multiplier rate, $\dot{\mu}$:

$$\dot{\varepsilon} = \dot{\mu}\frac{\partial\psi(\boldsymbol{\sigma})}{\partial\boldsymbol{\sigma}}. \tag{12}$$

Therefore, the power of dissipation can be formulated as a function of strain rates for each domain presented in [61]:

$$D(\dot{\boldsymbol{\varepsilon}}) = c'.A_i.t_i.\cos\phi', \tag{13}$$

where $A_i$ is the area of the element of node $i$, $t_i$ is a vector of additional variables defined by:

$$\|\boldsymbol{\rho}\|_i \leq t_i, \tag{14}$$

$$\boldsymbol{\rho}_i = \begin{bmatrix} \rho_1 \\ \rho_2 \end{bmatrix} = \begin{bmatrix} \dot{\varepsilon}_{xx} - \dot{\varepsilon}_{yy} \\ \dot{\gamma}_{xy} \end{bmatrix}. \tag{15}$$

The change volume after deformation in cohesive-frictional soil can be calculated from:

$$\dot{\varepsilon}_{xx} + \dot{\varepsilon}_{yy} = t_i \sin\phi'. \tag{16}$$

Introducing an approximation of the displacement and the smoothed strains rates $\dot{\bar{\varepsilon}}_i$ can be calculated from Eq. (7), and the upper-bound limit analysis problem for plane strain using NS-FEM can be determined by minimizing the objective function as follows:

$$\frac{\sigma_s}{c'} = \lambda^+ = \min\left(\sum_{i=1}^{N_n} c'.A_i.t_i\cos\phi'\right), \tag{17}$$

$$st\begin{cases} \dot{u} = 0 \quad \text{on} \quad \Gamma_u \\ W_{\text{ext}}(\dot{u}) = 1 \\ \dot{\bar{\varepsilon}}_{xx} + \dot{\bar{\varepsilon}}_{yy} = t_i \sin\phi' \\ t_i \geq \sqrt{(\dot{\bar{\varepsilon}}_{xx} - \dot{\bar{\varepsilon}}_{yy})^2 + \dot{\bar{\gamma}}_{xy}^2}, \; i = 1, 2, \ldots\ldots, N_n \end{cases} \tag{18}$$

where $N_n$ is the total number of nodes in domain.

## 5. Numerical results

Due to symmetry, only half of domain is considered in this study. In this paper, GiD [62] is employed for automatic mesh generation with three node triangular elements. The size of domain is chosen sufficiently large enough to ensure that the failure mechanism only takes place inside the considered domain. For the case of $H/B = 1$ and $S/B = 2$, the domain was discretized into 4222 triangular elements as shown in Figure 3. The computations were performed on a Dell Optiplex 990 (Intel Core$^{\text{TM}}$ i7, 3.4GHz CPU, 8GB RAM) in Window XP environment using the conic interior-point optimizer of the Mosek package [60] mentioned above. The reported CPU times refer to the time actually spent on the interior-point iterations, i.e. they exclude the time taken to read the data file and execute a presolve routine with the aim of detecting and removing linearly dependent constraints.

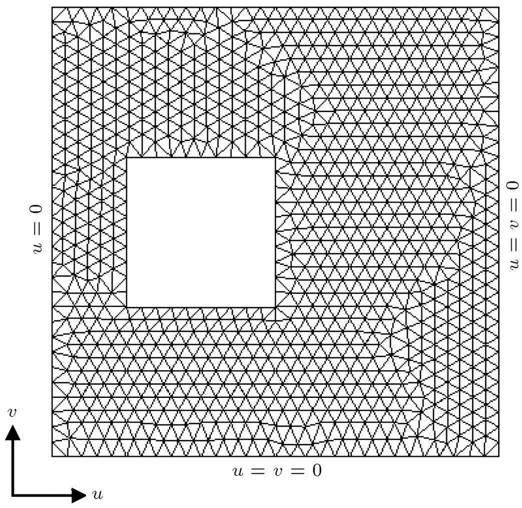


**Figure 3.** Typical mesh for dual square tunnels ($H/B = 1$, $S/B = 2$).

In order to find the collapse load, the details of the rigid-block mechanism were presented by Chen [63]. Subsequently, the upper bound rigid-block analysis of dual square tunnels subjected to surcharge loading was summarized by the study of Yamamoto et al. [27].

In this paper, the power dissipations of dual square tunnels using NS-FEM and SOCP are shown in Figures 4-7. Figures 4(b), 5(b), 6(b), and 7(b) show that the failure mechanisms indicated by the rigid blocks technique agree well with those derived from power dissipations using NS-FEM.

Figure 4(a) shows the power dissipation of dual square tunnels for shallow tunnel in the case of small friction angle, $\phi'$, and a close centre-to-centre spacing, $S/B$. It is noticeable that a small slip failure occurs between dual tunnels, and a large failure mechanism from the outside top corners of the tunnel extends up to the ground surface. Figure 5(a) shows the case for shallow depth, moderate friction angle, $\phi'$, and small

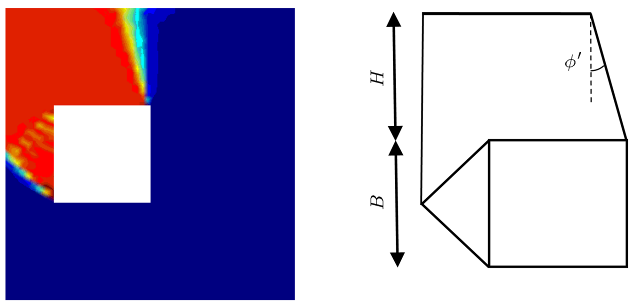


$\sigma_s/c' = 0.44$

(a) Power dissipation

$\sigma_s/c' = 0.42$

(b) Rigid-block mechanism

**Figure 4.** Comparison of rigid-block mechanism with NS-FEM limit analysis ($H/B = 1$, $\gamma B/c' = 1$, $S/B = 2$, $\phi' = 10°$, smooth interface).

distance between dual tunnels, $S/B$. In this figure, a small slip surface between two square tunnels enlarges to the top and bottom of tunnels, and a large surface

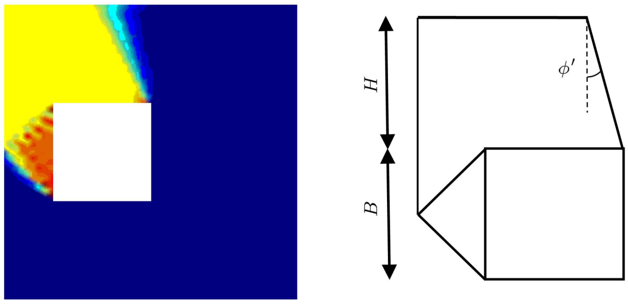


$\sigma_s/c' = 0.95$ $\sigma_s/c' = 0.88$

(a) Power dissipation (b) Rigid-block mechanism

**Figure 5.** Comparison of rigid-block mechanism with NS-FEM limit analysis ($H/B = 1$, $\gamma B/c' = 1$, $S/B = 2$, and $\phi' = 20°$, smooth interface).

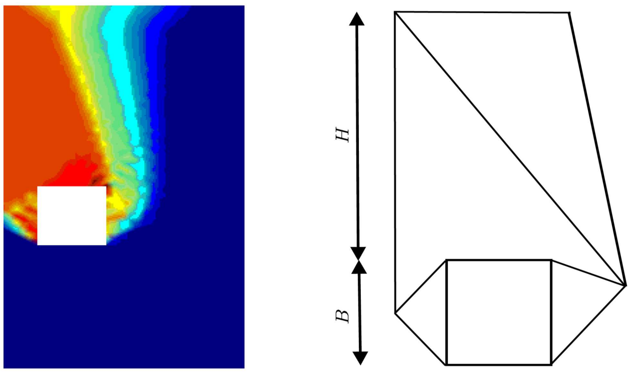


$\sigma_s/c' = 0.07$ $\sigma_s/c' = 0.17$

(a) Power dissipation (b) Rigid-block mechanism

**Figure 6.** Comparison of rigid-block mechanism with NS-FEM limit analysis ($H/B = 3$, $\gamma B/c' = 1$, $S/B = 2$, and $\phi' = 10°$, smooth interface).

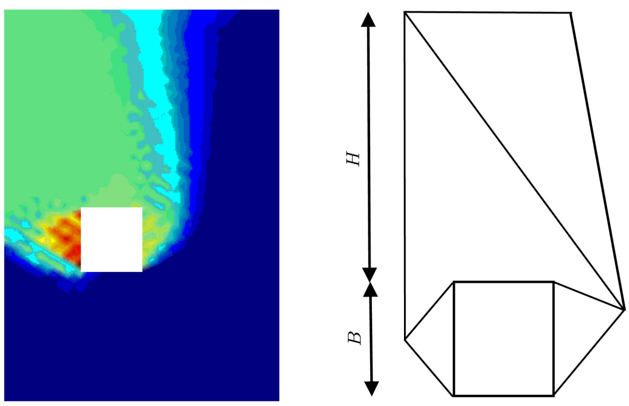


$\sigma_s/c' = 0.67$ $\sigma_s/c' = 1.25$

(a) Power dissipation (b) Rigid-block mechanism

**Figure 7.** Comparison of rigid-block mechanism with NS-FEM limit analysis ($H/B = 3$, $\gamma B/c' = 1$, $S/B = 3.5$, and $\phi' = 10°$, smooth interface).

from the outside top corners of the tunnel extends up to the ground surface.

Figure 6(a) shows the case for a moderate depth, small friction angle, $\phi'$, and a close centre-to-centre spacing, $S/B$. In this figure, a small slip surface between the tunnels enlarges to the top and bottom of tunnels and a large surface originates from the bottom of the tunnel extending up to the ground surface. Figure 7(a) shows the failure mechanism for tunnels of moderate depth with small friction angle, $\phi'$, and a moderate centre-to-centre spacing, $S/B$; the slip surface extends farther around bottom of the tunnel.

From what is shown in Figures 4-7, it is noticeable that the failure mechanism expands larger in both vertical and horizontal directions when ratios $H/B$ and $S/B$ increase. In addition, the distance between two tunnels (the ratio $S/B$) has a major influence on the stability of tunnels. The failure mechanisms from this proposed numerical procedure are identical to those of rigid block approach and solution of Yamamoto et al. [27]. The values of stability numbers from rigid-block mechanism are slightly greater than those from NS-FEM upper-bound solution. The numbers of stability errors calculated from NS-FEM and upper bound limit analysis based on the study of Yamamoto et al. [27] in the cases shown in Figures 4-7 are 2.29%, 1.06%, 25%, and 1.48%, respectively.

The influence of the distance of two tunnels and the results obtained are plotted in Figure 8. In the model analysed, the value of friction angle is $\phi' = 100$, and tunnels' depth varies ($H/B = 1$, 3, 5). In Figure 8, the failure mechanism of dual square tunnels is similar to that of single tunnel when it works independently. This proves that they do not influence one another when the distance between the two tunnels exceeds a certain value.

To evaluate the accuracy of this method, the stability numbers of the present method compared with those of Yamamoto et al. [27] are shown in Figures 9-11. From these figures, it is reasonable to conclude that the solutions are very reliable and accurate, because they are between the upper bound and lower bound's solutions derived from Yamamoto et al. [27]. In general, stability numbers decrease when $\gamma B/c'$ increases. Figures 10 and 11 present the stability numbers for the cases of $H/B = 3$, and $H/B = 5$. In these figure, the stability numbers slightly decrease when $S/B$ increases from 1.25 to 3.0. This is because of the fact that when the two square tunnels are very close to each other, the extra resistance gained by increasing the width of the pillar is not enough to be the counterbalance of the extra soil mass that it must support.

The values of stability numbers using NS-FEM and SOCP are summarized in Table 1. For given values of $H/B$, there are the points where spacing between

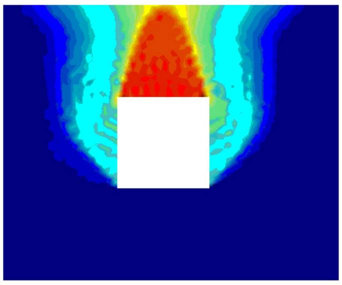

(a) Power dissipation ($H/B = 1$, $\gamma B/c' = 1$, $S/B = 3.5$, $\phi' = 10°$)

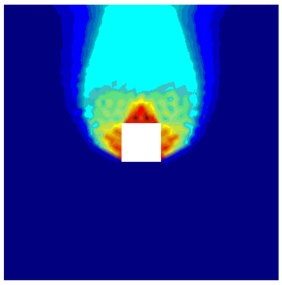

(b) Power dissipation ($H/B = 3$, $\gamma B/c' = 1$, $S/B = 7$, $\phi' = 10°$)

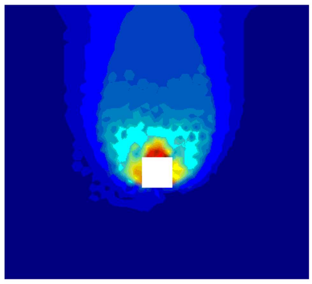

(c) Power dissipation ($H/B = 5$, $\gamma B/c' = 1$, $S/B = 10$, $\phi' = 10°$)

**Figure 8.** Numerical results from NS-FEM limit analysis (smooth interface).

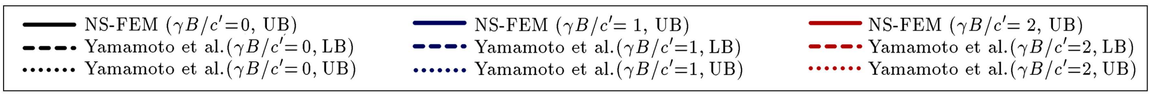


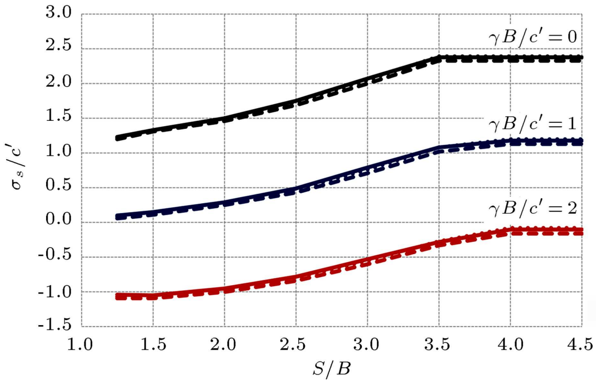


(a) $\phi' = 5°$

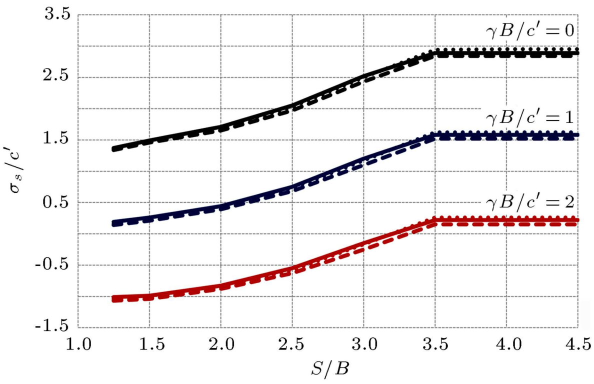


(b) $\phi' = 10°$

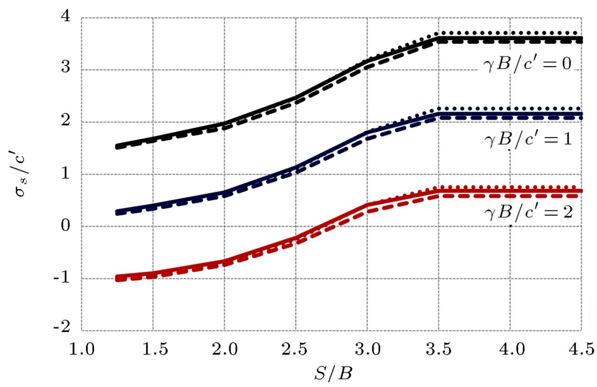


(c) $\phi' = 15°$

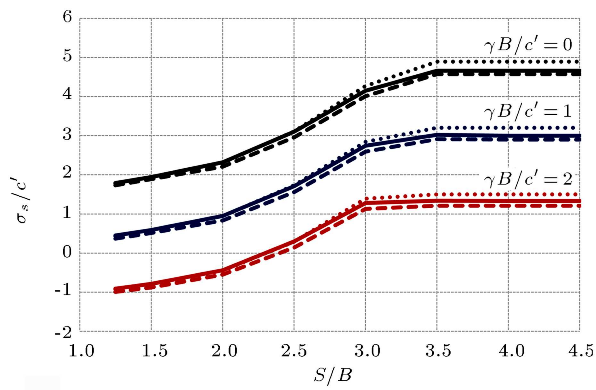


(d) $\phi' = 20°$

**Figure 9.** Comparisons of the stability numbers between the present method and that of Yamamoto et al. [27]. For the case $H/B = 1$, smooth interface: (a) $\phi' = 5°$, (b) $\phi' = 10°$, (c) $\phi' = 15°$, and (d) $\phi' = 20°$.

tunnels exceeds a certain value, and the stability load factors tend to become constant. The stability numbers at the no-interaction points for dual square tunnels are highlighted in bold. In cases of $H/B = 5$ and $\gamma B/c' = 3$, the stability numbers close to zero are indicated by "-", meaning that the tunnels collapse under the weight of the soil.

It is important to consider the meaning of the stability. The negative results imply that a tensile normal stress can be applied to the ground surface to ensure that no collapse will occur, but this cannot be seen in engineering practice. The positive ones imply that the tunnel will collapse when it is subjected to a compressive stress on the ground surface of such a value.

The efficiency of this upper bound procedure was also examined. The data are illustrated in Figure 12 where the numerical procedure based on NS-FEM gives the results with the rapid convergence. Particularly, the results here are much better (significant lower)

**Table 1.** The comparison between the present results and those of Yamamoto et al. [27] (for smooth interface).

| $H/B$ | $\phi'$ | $S/B$ | $\gamma B/c' = 0$ | | | $\gamma B/c' = 1$ | | | $\gamma B/c' = 2$ | | | $\gamma B/c' = 3$ | | |
|---|---|---|---|---|---|---|---|---|---|---|---|---|---|---|
| | | | NS-FEM | [27] | | NS-FEM | [27] | | NS-FEM | [27] | | NS-FEM | [27] | |
| | | | | LB | UB | | LB | UB | | LB | UB | | LB | UB |
| 1 | 5 | 1.25 | 1.23 | 1.20 | 1.22 | 0.10 | 0.06 | 0.08 | -1.04 | -1.09 | -1.07 | -2.18 | -2.24 | -2.21 |
| | | 1.50 | 1.33 | 1.31 | 1.32 | 0.15 | 0.11 | 0.13 | -1.05 | -1.09 | -1.07 | -2.26 | -2.30 | -2.28 |
| | | 2.00 | 1.50 | 1.46 | 1.49 | 0.29 | 0.25 | 0.28 | -0.95 | -1.00 | -0.97 | -2.22 | -2.26 | -2.23 |
| | | 2.50 | 1.75 | 1.69 | 1.73 | 0.49 | 0.43 | 0.47 | -0.78 | -0.84 | -0.80 | -2.09 | -2.14 | -2.09 |
| | | 3.00 | 2.07 | 2.00 | 2.05 | 0.79 | 0.71 | 0.76 | -0.53 | -0.60 | -0.55 | -1.90 | -1.96 | -1.90 |
| | | 3.50 | **2.38** | **2.33** | **2.39** | 1.08 | 1.02 | 1.08 | -0.28 | -0.33 | -0.27 | -1.66 | -1.72 | -1.65 |
| | | 4.00 | 2.38 | 2.33 | 2.39 | **1.18** | **1.13** | **1.20** | **-0.10** | **-0.16** | **-0.08** | **-1.44** | **-1.50** | **-1.43** |
| | | 4.50 | 2.38 | 2.33 | 2.39 | 1.18 | 1.13 | 1.20 | -0.10 | -0.16 | -0.08 | -1.44 | -1.50 | -1.43 |
| | 10 | 1.25 | 1.37 | 1.34 | 1.36 | 0.19 | 0.14 | 0.16 | -1.01 | -1.07 | -1.04 | -2.21 | -2.27 | -2.25 |
| | | 1.50 | 1.49 | 1.46 | 1.48 | 0.26 | 0.21 | 0.25 | -0.99 | -1.04 | -1.01 | -2.25 | -2.30 | -2.27 |
| | | 2.00 | 1.71 | 1.65 | 1.69 | 0.44 | 0.39 | 0.43 | -0.83 | -0.88 | -0.85 | -2.12 | -2.18 | -2.14 |
| | | 2.50 | 2.05 | 1.97 | 2.03 | 0.75 | 0.68 | 0.73 | -0.55 | -0.63 | -0.58 | -1.88 | -1.95 | -1.90 |
| | | 3.00 | 2.52 | 2.43 | 2.50 | 1.20 | 1.10 | 1.17 | -0.15 | -0.25 | -0.17 | -1.53 | -1.62 | -1.54 |
| | | 3.50 | **2.89** | **2.84** | **2.94** | **1.58** | **1.52** | **1.62** | **0.22** | **0.15** | **0.26** | **-1.18** | **-1.25** | **-1.15** |
| | | 4.00 | 2.89 | 2.84 | 2.95 | 1.58 | 1.52 | 1.62 | 0.22 | 0.15 | 0.26 | -1.18 | -1.25 | -1.15 |
| | | 4.50 | 2.89 | 2.84 | 2.95 | 1.58 | 1.52 | 1.62 | 0.22 | 0.15 | 0.26 | -1.18 | -1.25 | -1.15 |
| | 15 | 1.25 | 1.55 | 1.51 | 1.53 | 0.29 | 0.24 | 0.28 | -0.96 | -1.03 | -1.00 | -2.24 | -2.31 | -2.27 |
| | | 1.50 | 1.68 | 1.64 | 1.68 | 0.40 | 0.34 | 0.39 | -0.90 | -0.97 | -0.93 | -2.22 | -2.29 | -2.25 |
| | | 2.00 | 1.97 | 1.88 | 1.96 | 0.65 | 0.58 | 0.64 | -0.67 | -0.74 | -0.69 | -2.00 | -2.08 | -2.02 |
| | | 2.50 | 2.47 | 2.37 | 2.46 | 1.13 | 1.03 | 1.11 | -0.22 | -0.33 | -0.25 | -1.59 | -1.70 | -1.62 |
| | | 3.00 | 3.17 | 3.05 | 3.19 | 1.80 | 1.68 | 1.81 | 0.41 | 0.28 | 0.41 | -1.01 | -1.14 | -1.01 |
| | | 3.50 | **3.61** | **3.54** | **3.71** | **2.16** | **2.08** | **2.26** | **0.68** | **0.58** | **0.75** | **-0.83** | **-0.94** | **-0.78** |
| | | 4.00 | 3.61 | 3.54 | 3.71 | 2.16 | 2.08 | 2.26 | 0.68 | 0.58 | 0.75 | -0.83 | -0.94 | -0.78 |
| | | 4.50 | 3.61 | 3.54 | 3.71 | 2.16 | 2.08 | 2.26 | 0.68 | 0.58 | 0.75 | -0.83 | -0.94 | -0.78 |
| | 20 | 1.25 | 1.79 | 1.73 | 1.78 | 0.45 | 0.37 | 0.43 | -0.91 | -0.99 | -0.93 | -2.27 | -2.35 | -2.30 |
| | | 1.50 | 1.94 | 1.89 | 1.94 | 0.59 | 0.51 | 0.58 | -0.79 | -0.88 | -0.81 | -2.19 | -2.28 | -2.22 |
| | | 2.00 | 2.32 | 2.21 | 2.31 | 0.95 | 0.83 | 0.94 | -0.44 | -0.55 | -0.45 | -1.84 | -1.94 | -1.84 |
| | | 2.50 | 3.10 | 2.96 | 3.11 | 1.71 | 1.56 | 1.73 | 0.30 | 0.14 | 0.29 | -1.13 | -1.29 | -1.16 |
| | | 3.00 | 4.15 | 4.01 | 4.27 | 2.74 | 2.59 | 2.84 | 1.28 | 1.13 | 1.39 | -0.35 | **-0.53** | **-0.26** |
| | | 3.50 | **4.66** | **4.57** | **4.89** | **3.02** | **2.91** | **3.20** | **1.34** | **1.21** | **1.50** | **-0.38** | -0.53 | -0.26 |
| | | 4.00 | 4.66 | 4.57 | 4.89 | 3.00 | 2.90 | 3.20 | 1.33 | 1.21 | 1.50 | -0.38 | -0.53 | -0.26 |
| | | 4.50 | 4.66 | 4.57 | 4.89 | 3.00 | 2.90 | 3.20 | 1.33 | 1.21 | 1.50 | -0.38 | -0.53 | -0.26 |
| 3 | 5 | 1.25 | 3.32 | 3.28 | 3.35 | -0.18 | -0.23 | -0.16 | -3.71 | -3.77 | -3.72 | -7.26 | -7.35 | -7.29 |
| | | 1.50 | 3.22 | 3.19 | 3.26 | -0.27 | -0.32 | -0.25 | -3.81 | -3.87 | -3.81 | -7.38 | -7.45 | -7.39 |
| | | 2.00 | 3.10 | 3.05 | 3.12 | -0.38 | -0.44 | -0.37 | -3.89 | -3.97 | -3.90 | -7.44 | -7.54 | -7.47 |
| | | 2.50 | 3.13 | 3.04 | 3.12 | -0.35 | -0.45 | -0.37 | -3.85 | -3.97 | -3.89 | -7.40 | -7.51 | -7.44 |
| | | 3.00 | 3.26 | 3.15 | 3.24 | -0.23 | -0.34 | -0.25 | -3.74 | -3.86 | -3.78 | -7.30 | -7.42 | -7.34 |
| | | 3.50 | 3.43 | 3.33 | 3.42 | -0.06 | -0.17 | -0.07 | -3.59 | -3.70 | -3.61 | -7.16 | -7.26 | -7.17 |
| | | 4.00 | 3.61 | 3.53 | 3.63 | 0.11 | 0.03 | 0.13 | -3.42 | -3.51 | -3.41 | -6.99 | -7.09 | -6.99 |
| | | 4.50 | 3.78 | 3.72 | 3.84 | 0.28 | 0.22 | 0.33 | -3.26 | -3.33 | -3.22 | - -6.83 | -6.92 | -6.81 |
| | | 5.00 | 3.97 | 3.90 | 4.02 | 0.47 | 0.39 | 0.51 | -3.07 | -3.16 | -3.05 | -6.65 | -6.75 | -6.63 |
| | | 5.50 | 4.11 | 4.06 | 4.18 | 0.62 | 0.55 | 0.68 | -2.92 | -3.00 | -2.87 | -6.49 | -6.58 | -6.45 |
| | | 6.00 | 4.27 | 4.20 | 4.34 | 0.77 | 0.70 | 0.83 | -2.76 | -2.84 | -2.71 | -6.33 | **-6.42** | **-6.28** |
| | | 6.50 | 4.39 | 4.33 | 4.48 | 0.89 | 0.83 | 0.98 | -2.64 | **-2.71** | **-2.56** | **-6.27** | -6.42 | -6.28 |

**Table 1.** The comparison between the present results and those of Yamamoto et al. [27] (for smooth interface) (continued).

| $H/B$ | $\phi'$ | $S/B$ | $\gamma B/c'=0$ | | | $\gamma B/c'=1$ | | | $\gamma B/c'=2$ | | | $\gamma B/c'=3$ | | |
|---|---|---|---|---|---|---|---|---|---|---|---|---|---|---|
| | | | NS-FEM | [27] | | NS-FEM | [27] | | NS-FEM | [27] | | NS-FEM | [27] | |
| | | | | LB | UB | | LB | UB | | LB | UB | | LB | UB |
| | | 7.00 | 4.52 | 4.46 | 4.62 | 1.02 | **0.96** | **1.11** | **–2.57** | –2.71 | –2.56 | –6.27 | –6.42 | –6.28 |
| | | 7.50 | **4.69** | **4.58** | **4.76** | **1.08** | 0.96 | 1.11 | –2.57 | –2.71 | –2.56 | –6.27 | –6.42 | –6.28 |
| | | 8.00 | 4.69 | 4.58 | 4.76 | 1.08 | 0.96 | 1.11 | –2.57 | –2.71 | –2.56 | –6.27 | –6.42 | –6.28 |
| | | 8.50 | 4.69 | 4.58 | 4.76 | 1.08 | 0.96 | 1.11 | –2.57 | –2.71 | –2.56 | –6.27 | –6.42 | –6.28 |
| | 10 | 1.25 | 4.21 | 4.17 | 4.28 | 0.33 | 0.26 | 0.37 | –3.71 | –3.72 | –3.61 | – | – | – |
| | | 1.50 | 4.08 | 4.04 | 4.14 | 0.21 | 0.15 | 0.26 | –3.74 | –3.84 | –3.73 | – | – | – |
| | | 2.00 | 3.87 | 3.79 | 3.91 | 0.07 | –0.02 | 0.09 | –3.79 | –3.92 | –3.80 | – | – | – |
| | | 2.50 | 3.91 | 3.78 | 3.90 | 0.15 | 0.01 | 0.13 | –3.65 | –3.82 | –3.69 | – | – | – |
| | | 3.00 | 4.10 | 3.95 | 4.09 | 0.39 | 0.22 | 0.36 | –3.37 | –3.55 | –3.41 | – | – | – |
| | | 3.50 | 4.36 | 4.23 | 4.39 | 0.67 | 0.52 | 0.68 | –3.07 | –3.22 | –3.07 | – | – | – |
| | | 4.00 | 4.63 | 4.54 | 4.72 | 0.95 | 0.86 | 1.02 | –2.77 | –2.87 | -2.71 | – | – | – |
| | | 4.50 | 4.89 | 4.82 | 5.01 | 1.22 | 1.14 | 1.33 | –2.50 | –2.59 | –2.41 | – | – | – |
| | | 5.00 | 5.16 | 5.07 | 5.27 | 1.50 | 1.39 | 1.60 | –2.22 | –2.36 | –2.16 | – | – | – |
| | | 5.50 | 5.37 | 5.29 | 5.53 | 1.71 | 1.62 | 1.85 | –2.02 | **–2.13** | **–1.92** | – | – | – |
| | | 6.00 | 5.63 | 5.51 | 5.75 | 1.96 | 1.85 | 2.10 | **–1.94** | –2.13 | –1.92 | – | – | – |
| | | 6.50 | 5.82 | 5.74 | 5.99 | 2.16 | **2.06** | **2.32** | –1.94 | –2.13 | –1.92 | – | – | – |
| | | 7.00 | 6.06 | 5.95 | 6.24 | **2.22** | 2.06 | 2.32 | –1.94 | –2.13 | –1.92 | – | – | – |
| | | 7.50 | 6.26 | **6.17** | **6.44** | 2.22 | 2.06 | 2.32 | –1.94 | –2.13 | –1.92 | – | – | – |
| | | 8.00 | **6.30** | 6.17 | 6.44 | 2.22 | 2.06 | 2.32 | -1.94 | –2.13 | –1.92 | – | – | – |
| | | 8.50 | 6.30 | 6.17 | 6.44 | 2.22 | 2.06 | 2.32 | –1.94 | –2.13 | –1.92 | – | – | – |
| | 15 | 1.25 | 5.57 | 5.50 | 5.70 | 1.11 | 1.00 | 1.18 | –3.63 | – | – | – | – | – |
| | | 1.50 | 5.37 | 5.29 | 5.49 | 0.96 | 0.86 | 1.05 | –3.79 | – | – | – | – | – |
| | | 2.00 | 5.04 | 4.90 | 5.10 | 0.79 | 0.63 | 0.83 | –3.71 | – | – | – | – | – |
| | | 2.50 | 5.08 | 4.87 | 5.10 | 0.95 | 0.73 | 0.95 | –3.29 | –2.98 | –2.75 | – | – | – |
| | | 3.00 | 5.37 | 4.87 | 5.42 | 1.34 | 1.12 | 1.36 | –2.73 | –2.98 | –2.75 | – | – | – |
| | | 3.50 | 5.80 | 5.16 | 5.92 | 1.83 | 1.65 | 1.93 | –2.19 | –2.38 | –2.13 | – | – | – |
| | | 4.00 | 6.20 | 5.62 | 6.43 | 2.25 | 2.11 | 2.44 | –1.78 | –1.95 | –1.64 | – | – | – |
| | | 4.50 | 6.60 | 6.09 | 6.89 | 2.66 | 2.54 | 2.91 | –1.41 | –1.19 | –1.22 | – | – | – |
| | | 5.00 | 7.04 | 6.86 | 7.27 | 3.14 | 2.95 | 3.38 | –0.94 | –1.05 | –0.81 | – | – | – |
| | | 5.50 | 7.38 | 7.25 | 7.72 | 3.48 | 3.33 | 3.81 | –0.79 | **–1.13** | **–0.63** | – | – | – |
| | | 6.00 | 7.85 | 7.64 | 8.15 | 3.94 | 3.72 | 4.21 | **–0.80** | –1.13 | –0.63 | – | – | – |
| | | 6.50 | 8.21 | 8.04 | 8.58 | **4.22** | **3.98** | **4.48** | –0.80 | –1.13 | –0.63 | – | – | – |
| | | 7.00 | 8.64 | 8.45 | 9.02 | 4.22 | 3.98 | 4.48 | –0.80 | –1.13 | –0.63 | – | – | – |
| | | 7.50 | **9.02** | **8.83** | **9.38** | 4.22 | 3.98 | 4.48 | –0.80 | –1.13 | –0.63 | – | – | – |
| | | 8.00 | 9.02 | 8.83 | 9.38 | 4.22 | 3.98 | 4.48 | –0.80 | –1.13 | –0.63 | – | – | – |
| | | 8.50 | 9.02 | 8.83 | 9.38 | 4.22 | 3.98 | 4.48 | –0.80 | –1.13 | –0.63 | – | – | – |
| | 20 | 1.25 | 7.82 | 7.70 | 8.11 | 2.42 | 2.23 | 2.62 | – | – | – | – | – | – |
| | | 1.50 | 7.48 | 7.31 | 7.76 | 2.20 | 2.03 | 2.42 | – | – | – | – | – | – |
| | | 2.00 | 6.94 | 6.68 | 7.12 | 2.00 | 1.74 | 2.15 | – | – | – | – | – | – |

**Table 1.** The comparison between the present results and those of Yamamoto et al. [27] (for smooth interface) (continued).

| $H/B$ | $\phi'$ | $S/B$ | $\gamma B/c' = 0$ | | | $\gamma B/c' = 1$ | | | $\gamma B/c' = 2$ | | | $\gamma B/c' = 3$ | | |
|---|---|---|---|---|---|---|---|---|---|---|---|---|---|---|
| | | | NS-FEM | [27] | | NS-FEM | [27] | | NS-FEM | [27] | | NS-FEM | [27] | |
| | | | | LB | UB | | LB | UB | | LB | UB | | LB | UB |
| | | 2.50 | 6.96 | 6.62 | 7.09 | 2.29 | 1.96 | 2.37 | –2.54 | – | –2.56 | – | – | – |
| | | 3.00 | 7.42 | 7.14 | 7.73 | 2.97 | 2.66 | 3.20 | –1.56 | –1.89 | –1.39 | – | – | – |
| | | 3.50 | 8.16 | 7.91 | 8.58 | 3.78 | 3.51 | 4.10 | –0.74 | –1.07 | –0.51 | – | – | – |
| | | 4.00 | 8.79 | 8.60 | 9.38 | 4.46 | 4.24 | 4.98 | –0.09 | –0.39 | 0.29 | – | – | – |
| | | 4.50 | 9.46 | 9.26 | 10.14 | 5.16 | 4.96 | 5.80 | 0.56 | 0.29 | 1.00 | – | – | – |
| | | 5.00 | 10.28 | 9.95 | 10.88 | 6.04 | 5.66 | 6.60 | 1.40 | 0.96 | 1.80 | – | – | – |
| | 20 | 5.50 | 10.93 | 10.69 | 11.75 | 6.66 | 6.41 | 7.43 | **1.68** | **1.21** | **2.28** | – | – | – |
| | | 6.00 | 11.87 | 11.47 | 12.71 | 7.60 | 7.18 | 8.37 | 1.67 | 1.21 | 2.28 | – | – | – |
| | | 6.50 | 12.58 | 12.27 | 13.66 | 8.14 | **7.73** | **8.94** | 1.67 | 1.21 | 2.28 | – | – | – |
| | | 7.00 | 13.46 | 13.12 | 14.51 | **8.16** | 7.73 | 8.94 | 1.67 | 1.21 | 2.28 | – | – | – |
| | | 7.50 | **14.16** | **13.81** | **15.13** | 8.16 | 7.73 | 8.94 | 1.67 | 1.21 | 2.28 | – | – | – |
| | | 8.00 | 14.16 | 13.81 | 15.13 | 8.16 | 7.73 | 8.94 | 1.67 | 1.21 | 2.28 | – | – | – |
| | | 8.50 | 14.16 | 13.81 | 15.13 | 8.16 | 7.73 | 8.94 | 1.67 | 1.21 | 2.28 | – | – | – |
| 5 | 5 | 1.25 | 4.68 | 4.61 | 4.71 | –1.15 | –1.25 | –1.15 | –7.05 | –7.17 | –7.08 | – | – | – |
| | | 1.50 | 4.56 | 4.51 | 4.60 | –1.28 | –1.36 | –1.26 | –7.20 | –7.29 | –7.19 | – | – | – |
| | | 2.00 | 4.36 | 4.30 | 4.40 | –1.46 | –1.53 | –1.43 | –7.33 | –7.44 | –7.34 | – | – | – |
| | | 2.50 | 4.26 | 4.17 | 4.28 | –1.53 | –1.63 | –1.53 | –7.37 | –7.49 | –7.39 | – | – | – |
| | | 3.00 | 4.27 | 4.16 | 4.27 | –1.49 | –1.62 | –1.51 | –7.31 | –7.44 | –7.34 | – | – | – |
| | | 3.50 | 4.36 | 4.22 | 4.35 | –1.37 | –1.52 | –1.40 | –7.16 | –7.32 | –7.21 | – | – | – |
| | | 4.00 | 4.42 | 4.33 | 4.47 | –1.30 | –1.39 | –1.26 | –7.07 | –7.16 | –7.04 | – | – | – |
| | | 4.50 | 4.53 | 4.47 | 4.61 | –1.17 | –1.25 | –1.11 | –6.92 | –7.01 | –6.87 | – | – | – |
| | | 5.00 | 4.61 | 4.59 | 4.71 | –1.04 | –1.12 | –0.97 | –6.78 | –6.86 | –6.72 | – | – | – |
| | | 5.50 | 4.75 | 4.70 | 4.85 | –0.92 | –0.99 | –0.83 | –6.64 | –6.71 | –6.56 | – | – | – |
| | | 6.00 | 4.88 | 4.80 | 4.96 | –0.78 | –0.87 | –0.71 | –6.47 | –6.58 | –6.41 | – | – | – |
| | | 6.50 | 4.99 | 4.89 | 5.07 | –0.65 | –0.76 | –0.59 | –6.34 | –6.46 | –6.29 | – | – | – |
| | | 7.00 | 5.10 | 5.00 | 5.17 | –0.55 | –0.65 | –0.48 | –6.23 | –6.34 | –6.17 | – | – | – |
| | | 7.50 | 5.18 | 5.09 | 5.28 | –0.45 | –0.55 | –0.36 | –6.13 | –6.23 | –6.06 | – | – | – |
| | | 8.00 | 5.30 | 5.20 | 5.39 | –0.33 | –0.44 | –0.25 | –6.01 | –6.12 | –5.94 | – | – | – |
| | | 8.50 | 5.40 | 5.30 | 5.50 | –0.23 | –0.33 | –0.14 | –5.92 | –6.02 | –5.83 | – | – | – |
| | | 9.00 | 5.51 | 5.41 | 5.60 | –0.11 | –0.23 | –0.03 | –5.80 | –**5.93** | –**5.74** | – | – | – |
| | | 9.50 | 5.62 | 5.51 | 5.71 | –0.01 | –0.12 | 0.08 | –**5.75** | –5.93 | –5.74 | – | – | – |
| | | 10.00 | 5.72 | 5.61 | 5.83 | 0.09 | –0.02 | 0.18 | –5.75 | –5.93 | –5.74 | – | – | – |
| | | 10.50 | 5.82 | 5.71 | 5.93 | 0.19 | **0.07** | **0.29** | –5.75 | –5.93 | –5.74 | – | – | – |
| | | 11.00 | 5.92 | 5.81 | 6.03 | **0.25** | 0.07 | 0.29 | –5.75 | –5.93 | –5.74 | – | – | – |
| | | 11.50 | 6.02 | 5.90 | 6.12 | 0.25 | 0.07 | 0.29 | -5.75 | -5.93 | -5.74 | - | - | - |
| | | 12.00 | **6.12** | **6.00** | **6.24** | 0.25 | 0.07 | 0.29 | -5.75 | -5.93 | -5.74 | - | - | - |
| | | 12.50 | 6.12 | 6.00 | 6.24 | 0.25 | 0.07 | 0.29 | –5.75 | –5.93 | -5.74 | – | – | – |
| | 10 | 1.25 | 6.34 | 6.24 | 6.44 | –0.39 | –0.55 | –0.38 | – | – | – | – | – | – |
| | | 1.50 | 6.16 | 6.07 | 6.25 | –0.57 | –0.69 | –0.52 | – | – | – | – | – | – |
| | | 2.00 | 5.83 | 5.71 | 5.92 | –0.80 | –0.91 | –0.74 | – | – | – | – | – | – |

**Table 1.** The comparison between the present results and those of Yamamoto et al. [27] (for smooth interface) (continued).

| $H/B$ | $\phi'$ | $S/B$ | $\gamma B/c'=0$ | | | $\gamma B/c'=1$ | | | $\gamma B/c'=2$ | | | $\gamma B/c'=3$ | | |
|---|---|---|---|---|---|---|---|---|---|---|---|---|---|---|
| | | | NS-FEM | [27] | | NS-FEM | [27] | | NS-FEM | [27] | | NS-FEM | [27] | |
| | | | | LB | UB | | LB | UB | | LB | UB | | LB | UB |
| | | 2.50 | 5.67 | 5.52 | 5.72 | –0.84 | –1.00 | –0.83 | – | – | – | – | – | – |
| | | 3.00 | 5.67 | 5.49 | 5.71 | –0.72 | –0.91 | –0.72 | – | – | – | – | – | – |
| | | 3.50 | 5.81 | 5.60 | 5.83 | –0.47 | –0.70 | –0.49 | – | – | – | – | – | – |
| | | 4.00 | 5.89 | 5.79 | 6.03 | –0.33 | –0.43 | –0.21 | – | – | – | – | – | – |
| | | 4.50 | 6.06 | 5.97 | 6.20 | –0.10 | –0.19 | 0.05 | – | – | – | – | – | – |
| | | 5.00 | 6.21 | 6.13 | 6.41 | 0.10 | 0.01 | 0.28 | – | – | – | – | – | – |
| | | 5.50 | 6.37 | 6.28 | 6.59 | 0.30 | 0.22 | 0.49 | – | – | –5.71 | – | – | – |
| | | 6.00 | 6.58 | 6.45 | 6.77 | 0.54 | 0.59 | 0.92 | –5.60 | – | –5.48 | – | – | – |
| | | 6.50 | 6.80 | 6.61 | 6.93 | 0.79 | 0.79 | 1.11 | –5.36 | –5.56 | –5.29 | – | – | – |
| | | 7.00 | 6.97 | 6.80 | 7.12 | 0.97 | 0.79 | 1.11 | –5.23 | **–5.50** | **–5.17** | – | – | – |
| | | 7.50 | 7.14 | 6.98 | 7.34 | 1.15 | 0.98 | 1.33 | **–5.21** | –5.50 | –5.17 | – | – | – |
| | | 8.00 | 7.34 | 7.16 | 7.53 | 1.37 | 1.18 | 1.51 | –5.21 | –5.50 | –5.17 | – | – | – |
| | | 8.50 | 7.52 | 7.35 | 7.73 | 1.54 | 1.37 | 1.72 | –5.21 | –5.50 | –5.17 | – | – | – |
| | | 9.00 | 7.72 | 7.53 | 7.95 | 1.96 | 1.56 | 1.94 | –5.21 | –5.50 | –5.17 | – | – | – |
| | | 9.50 | 7.92 | 7.73 | 8.14 | **2.06** | **1.74** | **2.13** | –5.21 | –5.50 | –5.17 | – | – | – |
| | | 10.00 | 8.12 | 7.91 | 8.34 | 2.06 | 1.74 | 2.13 | –5.21 | –5.50 | –5.17 | – | – | – |
| | | 10.50 | 8.32 | 8.12 | 8.55 | 2.06 | 1.74 | 2.13 | –5.21 | –5.50 | –5.17 | – | – | – |
| | | 11.00 | 8.51 | 8.29 | 8.76 | 2.06 | 1.74 | 2.13 | –5.21 | –5.50 | –5.17 | – | – | – |
| | | 11.50 | 8.69 | 8.48 | 8.94 | 2.06 | 1.74 | 2.13 | –5.21 | –5.50 | –5.17 | – | – | – |
| | | 12.00 | **8.91** | **8.64** | **9.15** | 2.06 | 1.74 | 2.13 | –5.21 | –5.50 | –5.17 | – | – | – |
| | | 12.50 | 8.91 | 8.64 | 9.15 | 2.06 | 1.74 | 2.13 | –5.21 | –5.50 | –5.17 | – | – | – |
| | 15 | 1.25 | 9.21 | 9.03 | 9.41 | 1.00 | 0.73 | 1.10 | – | – | – | – | – | – |
| | | 1.50 | 8.78 | 8.70 | 9.08 | 0.72 | 0.51 | 0.87 | – | – | – | – | – | – |
| | | 2.00 | 8.29 | 8.07 | 8.50 | 0.39 | 0.16 | 0.50 | – | – | – | – | – | – |
| | | 2.50 | 8.06 | 7.78 | 8.21 | 0.45 | 0.15 | 0.52 | – | – | – | – | – | – |
| | | 3.00 | 8.03 | 7.74 | 8.21 | 0.70 | 0.40 | 0.80 | – | – | – | – | – | – |
| | | 3.50 | 8.25 | 7.93 | 8.39 | 1.17 | 0.83 | 1.27 | – | – | – | – | – | – |
| | | 4.00 | 8.33 | 8.19 | 8.68 | 1.39 | 1.23 | 1.70 | – | – | – | – | – | – |
| | | 4.50 | 8.58 | 8.43 | 8.98 | 1.75 | 1.58 | 2.08 | – | – | – | – | – | – |
| | | 5.00 | 8.81 | 8.66 | 9.25 | 2.10 | 1.94 | 2.48 | – | – | – | – | – | – |
| | | 5.50 | 9.09 | 8.94 | 9.57 | 2.44 | 2.29 | 2.83 | – | – | – | – | – | – |
| | | 6.00 | 9.46 | 9.23 | 9.88 | 2.87 | 2.65 | 3.26 | – | – | –3.76 | – | – | – |
| | | 6.50 | 9.91 | 9.56 | 10.21 | 3.36 | 3.01 | 3.64 | –3.72 | – | –3.52 | – | – | – |
| | | 7.00 | 10.24 | 9.90 | 10.63 | 3.71 | 3.37 | 4.05 | –3.75 | – | –3.55 | – | – | – |
| | | 7.50 | 10.56 | 10.26 | 10.96 | 4.03 | 3.74 | 4.47 | –3.72 | – | –3.49 | – | – | – |
| | | 8.00 | 10.95 | 10.63 | 11.43 | 4.45 | 4.13 | 4.87 | –3.79 | – | **–3.55** | – | – | – |
| | | 8.50 | 11.32 | 11.01 | 11.87 | 4.81 | 4.48 | 5.23 | **–3.74** | – | –3.55 | – | – | – |
| | | 9.00 | 11.69 | 11.39 | 12.25 | 5.18 | 4.85 | 5.69 | –3.74 | – | –3.55 | – | – | – |
| | | 9.50 | 12.09 | 11.76 | 12.70 | 5.46 | **5.20** | **6.05** | –3.74 | – | –3.55 | – | – | – |
| | | 10.00 | 12.53 | 12.16 | 13.41 | **5.64** | 5.20 | 6.05 | –3.74 | – | –3.55 | – | – | – |
| | | 10.50 | 12.94 | 12.54 | 13.62 | 5.64 | 5.20 | 6.05 | –3.74 | – | –3.55 | – | – | – |

**Table 1.** The comparison between the present results and those of Yamamoto et al. [27] (for smooth interface) (continued).

| $H/B$ | $\phi'$ | $S/B$ | $\gamma B/c' = 0$ | | | $\gamma B/c' = 1$ | | | $\gamma B/c' = 2$ | | | $\gamma B/c' = 3$ | | |
|---|---|---|---|---|---|---|---|---|---|---|---|---|---|---|
| | | | **NS-FEM** | **[27]** | | **NS-FEM** | **[27]** | | **NS-FEM** | **[27]** | | **NS-FEM** | **[27]** | |
| | | | | **LB** | **UB** | | **LB** | **UB** | | **LB** | **UB** | | **LB** | **UB** |
| | | 11.00 | 13.31 | 12.93 | 14.04 | 5.64 | 5.20 | 6.05 | –3.74 | – | –3.55 | – | – | – |
| | | 11.50 | 13.69 | 13.31 | 14.38 | 5.64 | 5.20 | 6.05 | –3.74 | – | –3.55 | – | – | – |
| | | 12.00 | **13.95** | 13.62 | 14.74 | 5.64 | 5.20 | 6.05 | –3.74 | – | –3.55 | – | – | – |
| | | 12.50 | 13.96 | 13.58 | 14.81 | 5.64 | 5.20 | 6.05 | –3.74 | – | –3.55 | – | – | – |
| | 20 | 1.25 | 14.70 | 14.38 | 15.42 | 3.92 | 3.41 | 4.26 | – | – | – | – | – | – |
| | | 1.50 | 14.02 | 13.66 | 14.74 | 3.44 | 3.00 | 3.80 | – | – | – | – | – | – |
| | | 2.00 | 12.88 | 12.42 | 13.44 | 2.88 | 2.41 | 3.23 | – | – | – | – | – | – |
| | | 2.50 | 12.53 | 11.98 | 13.07 | 3.17 | 2.58 | 3.42 | – | – | – | – | – | – |
| | | 3.00 | 12.47 | 12.01 | 13.16 | 3.69 | 3.21 | 4.23 | – | – | – | – | – | – |
| | | 3.50 | 12.80 | 12.24 | 13.40 | 4.47 | 3.84 | 4.89 | – | – | – | – | – | – |
| | | 4.00 | 12.79 | 12.52 | 13.70 | 4.74 | 4.43 | 5.52 | – | – | – | – | – | – |
| | | 4.50 | 13.15 | 12.85 | 14.20 | 5.36 | 5.03 | 6.21 | – | – | –2.21 | – | – | – |
| | | 5.00 | 13.59 | 13.28 | 14.71 | 5.98 | 5.66 | 7.06 | –2.14 | –2.54 | –1.44 | – | – | – |
| | | 5.50 | 14.14 | 13.83 | 15.44 | 6.65 | 6.32 | 7.64 | –1.43 | –1.85 | –0.55 | – | – | – |
| | | 6.00 | 14.87 | 14.45 | 16.07 | 7.43 | 7.03 | 8.58 | –0.75 | –1.16 | 0.18 | – | – | – |
| | | 6.50 | 15.84 | 15.14 | 16.99 | 8.47 | 7.78 | 9.44 | 0.10 | –0.58 | 0.96 | – | – | – |
| | | 7.00 | 16.56 | 15.90 | 17.87 | 9.25 | 8.52 | 10.20 | 0.76 | –0.14 | 1.57 | – | – | – |
| | | 7.50 | 17.25 | 16.67 | 18.60 | 9.91 | 9.34 | 11.01 | 1.05 | **–0.15** | **2.10** | – | – | – |
| | | 8.00 | 18.11 | 17.46 | 19.54 | 10.78 | 10.14 | 12.14 | 0.99 | –0.15 | 2.10 | – | – | – |
| | | 8.50 | 18.94 | 18.31 | 20.59 | 11.56 | 10.90 | 12.96 | 1.11 | –0.15 | 2.10 | – | – | – |
| | | 9.00 | 19.74 | 19.15 | 21.69 | 12.28 | 11.71 | 13.95 | **1.04** | –0.15 | 2.10 | – | – | – |
| | | 9.50 | 20.61 | 20.05 | 22.51 | 13.07 | 12.48 | 14.96 | 1.04 | –0.15 | 2.10 | – | – | – |
| | | 10.00 | 21.62 | 20.94 | 23.54 | 13.88 | **12.99** | **15.63** | 1.04 | –0.15 | 2.10 | – | – | – |
| | | 10.50 | 22.56 | 21.79 | 24.75 | **13.80** | 12.99 | 15.63 | 1.04 | –0.15 | 2.10 | – | – | – |
| | | 11.00 | 23.40 | 22.72 | 25.68 | 13.80 | 12.99 | 15.63 | 1.04 | –0.15 | 2.10 | – | – | – |
| | | 11.50 | 24.28 | 23.59 | 26.63 | 13.80 | 12.99 | 15.63 | 1.04 | –0.15 | 2.10 | – | – | – |
| | | 12.00 | **24.48** | **23.84** | **27.07** | 13.80 | 12.99 | 15.63 | 1.04 | –0.15 | 2.10 | – | – | – |
| | | 12.50 | 24.48 | 23.84 | 27.07 | 13.80 | 12.99 | 15.63 | 1.04 | -0.15 | 2.10 | – | – | – |

when compared with those from the upper bound analysis using finite-element method. Furthermore, this procedure used less than 4000 triangular elements (NS-FEM), but gave a better solution than that of Yamamoto et al. [27], in which 8072 triangular elements and 12105 stress/velocity discontinuities were used. In addition, adaptive techniques were also employed to refine meshes in [27]. The iterations and optimization Mosek times were also considered for the stability of the tunnel with $H/B = 3$, $S/B = 2$, and $\gamma B/c' = 1$. It is clear that the upper bound procedure based on NS-FEM reduces a dramatic number of variables in the optimisation problem in comparison with FEM upper bound analysis, especially when increasing the number of triangular elements in simulations. This leads to remarkably less time consumption by employing NS-FEM in upper bound procedure (Table 2).

## 6. Conclusions

An efficient procedure for upper bound limit analysis based on Node-based Smoothed Finite-Element

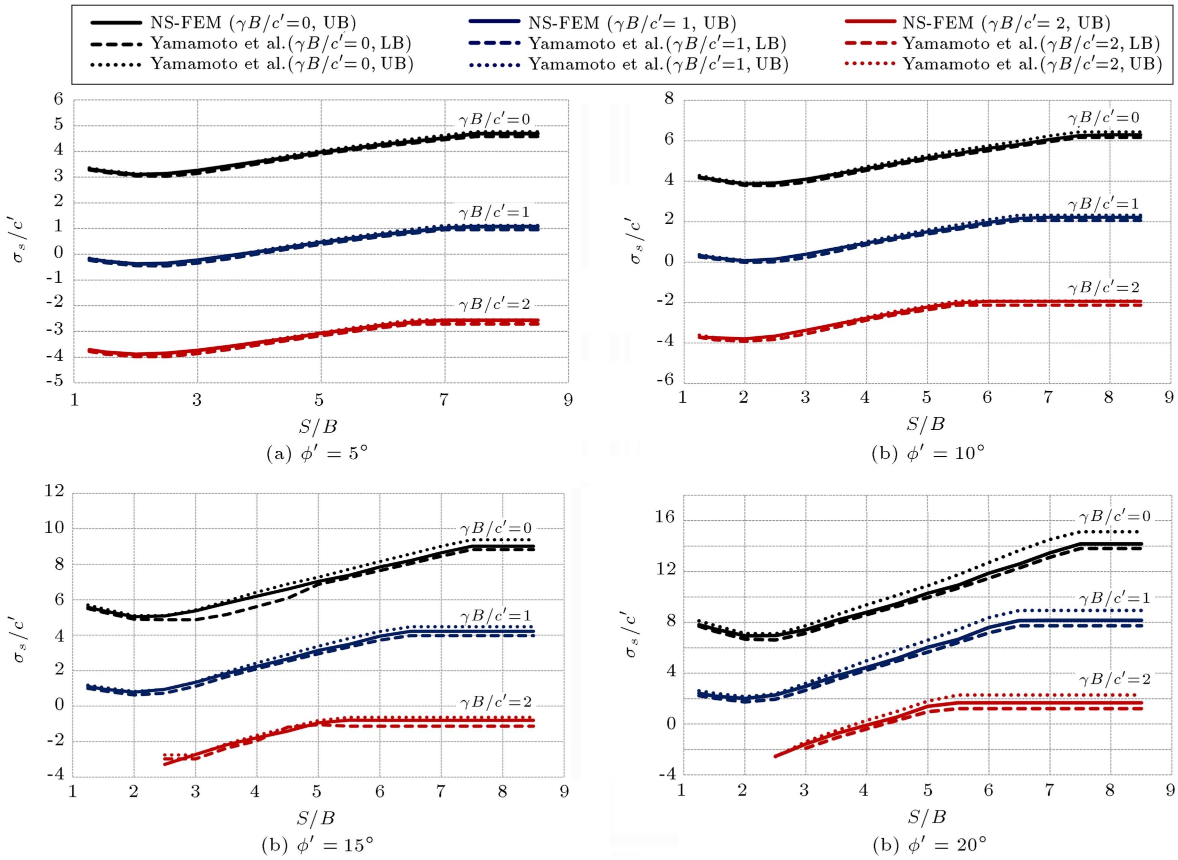


**Figure 10.** Comparisons of the stability numbers between the present method and that of Yamamoto et al. [27]. For the case $H/B = 3$, smooth interface: (a) $\phi' = 5°$, (b) $\phi' = 10°$, (c) $\phi' = 15°$, and (d) $\phi' = 20°$.

**Table 2.** The computational efficiency of the present method using NS-FEM and SOCP (for the case: $H/B = 3$, $\gamma B/c' = 1$, $S/B = 2$, and $\phi' = 5°$).

| | | | | | | | | |
|---|---|---|---|---|---|---|---|---|
| $\sigma_s/c'$ | NS-FEM | −0.2620 | −0.2962 | −0.3308 | −0.3388 | −0.3696 | −0.3793 | −0.3808 |
| | FEM | 1.6459 | 0.7988 | 0.5116 | 0.2935 | 0.1906 | 0.1578 | 0.0751 |
| $N_e$ | | 460 | 938 | 1480 | 2624 | 3752 | 4976 | 5920 |
| $N_{\text{var}}$ | NS-FEM | 1335 | 2605 | 4025 | 6980 | 9900 | 13040 | 15450 |
| | FEM | 1914 | 3856 | 6050 | 10664 | 15216 | 20144 | 23940 |
| Iteration | NS-FEM | 18 | 18 | 18 | 18 | 19 | 19 | 19 |
| | FEM | 18 | 20 | 20 | 21 | 21 | 21 | 21 |
| Mosek time (s) | NS-FEM | 0.55 | 0.81 | 1.14 | 2.42 | 4.51 | 5.01 | 7.33 |
| | FEM | 0.57 | 0.95 | 1.64 | 3.28 | 5.46 | 7.38 | 11.25 |

$N_e$ = no. of elements, $N_{\text{var}}$ = no. of variables

Method (NS-FEM) and Second-Order Cone Programming (SOCP) was described. Various numerical examples for dual square tunnels problem were presented to show that the present method can provide accurate and stable solutions with minimal computational effort. The obtained results are in well agreement with the average values of the lower and upper bounds reported by Yamamoto et al. [27]. Ratio $S/B$ plays an important role in the failure mechanism of dual square tunnels. When the spacing between two parallel tunnels is large

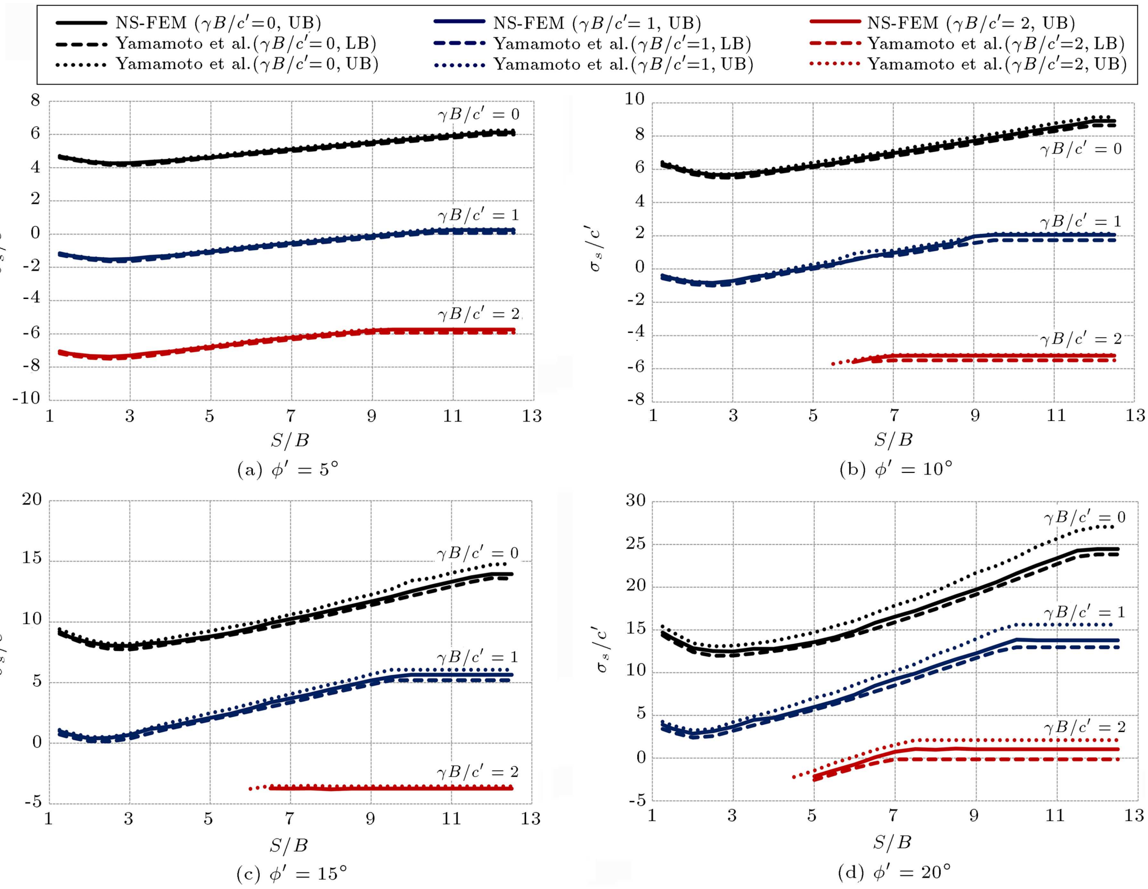


**Figure 11.** Comparisons of the stability numbers between the present method and that of Yamamoto et al. [27]. For the case $H/B = 5$, smooth interface: (a) $\phi' = 5°$, (b) $\phi' = 10°$, (c) $\phi' = 15°$, and (d) $\phi' = 20°$.

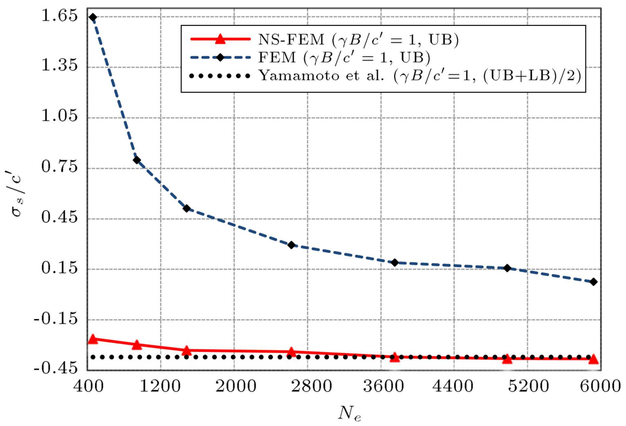


**Figure 12.** The convergence of stability numbers of dual square tunnels (for the case: $H/B = 3$, $S/B = 2$, $\gamma B/c' = 1$, and $\phi' = 5°$).

enough, the power dissipation and failure mechanism caused by each tunnel become independent.

The obtained solutions produced accurate and stable results for various cases of the given problem. In more complex and large-scale problems, when standard FEM models are easily faced with deterioration in the accuracy of results, NS-FEM might be useful due to its flexibility.


## Acknowledgments

This research was partially supported by the Foundation for Science and Technology at HCMUT University of Technology (Grant No. TNCS-2015-KTXD-09). We sincerely appreciate Dr. Canh V. Le for sharing the upper bound analysis code. This support is gratefully acknowledged.


## Nomenclature

| | |
|---|---|
| $B$ | The width of square tunnel |
| $H$ | Depth to the top of the tunnel |
| $S$ | The distance between the center of dual square tunnel |
| $c'$ | Cohesion of the soil |
| $\phi'$ | Friction angle of the soil |
| $\gamma$ | Unit weight of the soil |
| $\sigma_s$ | Surcharge loading distributed on the ground surface |
| $N_n$ | Total number of field nodes in the domain |
| $\tilde{\varepsilon}_k$ | Vector smoothing strain |

| | |
|---|---|
| $\Omega^{(k)}$ | Smoothing cells associated with the node $k$ |
| $\Phi_k(x)$ | Smoothing function |
| $A^{(k)}$ | Area of cell $\Omega^{(k)}$ |
| $\mathbf{d}_I$ | The nodal displacement vector |
| $\Gamma^{(k)}$ | Boundary of the domain $\Gamma^{(k)}$ |
| $\mathbf{n}^{(k)}$ | The outward normal vector matrix on the boundary $\Gamma^{(k)}$ |
| $\nabla_s \mathbf{u}$ | The symmetric gradient of the displacement field |
| $\tilde{\mathbf{B}}_I(\mathbf{x}_k)$ | The smoothed strain gradient matrix |
| $\mathbf{N_I}(\mathbf{x})$ | The shape function matrix |
| $\psi(\boldsymbol{\sigma})$ | The Mohr-Coulomb yield function |
| $\sigma_{xx}, \sigma_{yy}, \tau_{xy}$ | Normal and shear stresses defined with respect to a Cartesian |
| $\dot{\varepsilon}$ | Vector of plastic strain rates |
| $\dot{\mu}$ | The plastic multiplier |
| $\lambda^+$ | The stability numbers |
| $A_i$ | The area of the element of node $i$ |
| $t_i$ | Vector of additional variables |

## References


1. Murayama, S., Endo, M., Hashiba, T., Yamamoto, K., and Sasaki, H. (Eds.), "Geotechnical aspects for the excavating performance of the shield machines", In *The 21st Annual Lecture in Meeting of Japan Society of Civil Engineers* (1966).
2. Krause, T. "Shielding tunnel with liquid and earth-supported local chest" [Schildvortrieb mit Flüssigkeits- und erdgestützter ortsbrust], PhD Thesis, Technical University Carolo-Wilhelmina, Brunswick (1987).
3. Horn, N. "Horizontal earth pressure on the vertical surfaces of the tunnel tubes", In *National Conference of the Hungarian Civil Engineering Industry*, Budapest, pp. 7-16 (in German) (1961).
4. Davis, E.H., Gunn, M.J., Mair, R.J., and Seneviratne, H.N. "The stability of shallow tunnels and underground openings in cohesive material", *Geotechnique*, **30**(4), pp. 397-416 (1980).
5. Mühlhaus, H.B. "Lower bound solutions for circular tunnels in two and three dimensions", *Rock Mech Rock Eng.*, **18**, pp. 37-52 (1985).
6. Leca, E. and Dormieux, L. "Upper and lower bound solutions for the face stability of shallow circular tunnels in frictional material", *Geotechnique*, **40**(4), pp. 581-606 (1990).
7. Zhang, C., Han, K., and Zhang, D. "Face stability analysis of shallow circular tunnels in cohesive-frictional soils", *Tunnelling and Underground Space Technology*, **50**, pp. 345-357 (2015).
8. Atkinson, J.H. and Potts, D.M. "Stability of a shallow circular tunnel in cohesionless soils", *Géotechnique*, **27**(2), pp. 203-215 (1977).
9. Atkinson, J.H. and Cairncross, A.M. "Collapse of a shallow tunnel in a Mohr-Coulomb material", In *Role of Plasticity in Soil Mechanics*, Cambridge, pp. 202-206 (1973).
10. Cairncross, A.M. "Deformation around model tunnels in stiff clay", PhD Thesis, University of Cambridge (1973).
11. Seneviratne, H.N. "Deformations and pore-pressures around model tunnels in soft clay", PhD Thesis, University of Cambridge (1979).
12. Mair, R.J. "Centrifugal modelling of tunnel construction in soft clay", PhD Thesis, University of Cambridge (1979).
13. Chambon, P. and Corté, J.F. "Shallow tunnels in cohesionless soil: stability of tunnel face", *J. Geotech. Eng.*, **120**(7), pp. 1148-1165 (1994).
14. Kirsch, A. "Experimental investigation of the face stability of shallow tunnels in sand", *Acta. Geotech.*, **5**, pp. 43-62 (2010).
15. Idiger, G., Aklik, P., Wei, W., and Borja, I. "Centrifuge model test on the face stability of shallow tunnel", *Acta Geotech*, **6**, pp. 105-117 (2011).
16. Wu, B.R., and Lee, C.J. "Ground movements and collapse mechanisms induced by tunneling in clayey soil", *International Journal of Physical Modelling in Geotechnics*, **3**, pp. 15-29 (2003).
17. Chehade, F.H. and Shahrour, I. "Numerical analysis of the interaction between twin tunnels: influence of the relative position and construction procedure", *Tunnelling and Underground Space Technology*, **23**, pp. 210-214 (2008).
18. Osman, A.S. "Stability of unlined twin tunnels in undrained clay", *Tunnelling and Underground Space Technology*, **25**, pp. 290-296 (2010).
19. Mirhabibi, A. and Soroush, A. "Effects of surface buildings on twin tunnelling-induced ground settlements", *Tunnelling and Underground Space Technology*, **29**, pp. 40-51 (2012).
20. Sloan, S.W. and Assadi, A. "Undrained stability of a square tunnel in a soil whose strength increases linearly with depth", *Computers and Geotechnics*, **12**(4), pp. 321-346 (1991).
21. Lyamin, A.V. and Sloan, S.W. "Stability of a plane strain circular tunnel in a cohesive frictional soil", In: *Proceedings of the J.R. Booker Memorial Symposium*, Sydney, Australia, pp. 139-153 (2000).
22. Lyamin, A.V., Jack, D.L., and Sloan, S.W. "Collapse analysis of square tunnels in cohesive-frictional soils", In: *Proceedings of the First Asian-Pacific Congress on Computational Mechanics*, Sydney, Australia, pp. 405-414 (2001).

23. Yamamoto, K., Lyamin, A.V., Wilson, D.W., Sloan, S.W., and Abbo, A.J. "Stability of a single tunnel in cohesive-frictional soil subjected to surcharge loading", *Canadian Geotechnical Journal*, **48**(12), pp. 1841-1854 (2011).

24. Yamamoto, K., Lyamin, A.V., Wilson, D.W., Sloan, S.W., and Abbo, A.J. "Stability of a circular tunnel in cohesive-frictional soil subjected to surcharge loading", *Computers and Geotechnics*, **38**(4), pp. 504-514 (2011).

25. Sahoo, J.P. and Kumar, J. "Stability of long unsupported twin circular tunnels in soils", *Tunnelling and Underground Space Technology,* **38**, pp. 326-335 (2013).

26. Yamamoto, K., Lyamin, A.V., Wilson, D.W., Sloan, S.W., and Abbo, A.J. "Stability of dual circular tunnels in cohesive-frictional soil subjected to surcharge loading", *Computers and Geotechnics*, **50**, pp. 41-54 (2013).

27. Yamamoto, K., Lyamin, A.V., Wilson, D.W., Sloan, S.W., and Abbo, A.J. "Stability of dual square tunnels in cohesive-frictional soil subjected to surcharge loading", *Canadian Geotechnical Journal*, **51**, pp. 829-843 (2014).

28. Wilson, D.W., Abbo, A.J., Sloan, S.W., and Lyamin, A.V. "Undrained stability of dual square tunnels", *Acta Geotechnica*, **10**(5), pp. 665-682 (2015).

29. Wilson, D.W., Abbo, A.J., Sloan, S.W., and Lyamin, A.V. "Undrained stability of dual circular tunnels", *International Journal of Geomechanics*, **14**(1), pp. 69-79 (2014).

30. Hughes, T.J.R. "Reduced and selective integration techniques in the finite element analysis of plates", *Nuclear Engineering and Design*, **46**, pp. 203-222 (1978).

31. Hughes, T.J.R., *The Finite Element Method*, Dover Publications: Prentice-Hall (2000).

32. Piltner, R. and Taylor, R.L. "Triangular finite elements with rotational degrees of freedom and enhanced strain modes", *Computers and Structures*, **75,** pp. 361-368 (2000).

33. Simo, J.C. and Rifai, M.S. "A class of mixed assumed strain methods and the method of incompressible modes", *International Journal for Numerical Methods in Engineering*, **29**, pp. 1595-1638 (1990).

34. Cardoso, R.P.R., Yoon, J.W., Mahardika, M., Choudhry, S., Alves de Sousa, R.J., and Fontes Valente, R.A. "Enhanced assumed strain (EAS) and assumed natural strain (ANS) methods for one-point quadrature solid-shell elements", *International Journal for Numerical Methods in Engineering*, **75**, pp. 156-187 (2008).

35. Bonet, J. and Burton, A.J. "A simple average nodal pressure tetrahedral element for incompressible and nearly incompressible dynamic explicit applications", *Communications in Numerical Methods in Engineering*, **14**, pp. 437-449 (1998).

36. Chen, J.S., Wu, C.T., and Yoon, S. "A stabilized conforming nodal integration for Galerkin meshfree method", *International Journal for Numerical Methods in Engineering*, **50**, pp. 435-466 (2001).

37. Yoo, J.W., Moran, B., and Chen, J.S. "Stabilized conforming nodal integration in the natural-element method", *International Journal for Numerical Methods in Engineering*, **60**, pp. 861-890 (2004).

38. Liu, G.R. and Nguyen-Thoi, T., *Smoothed Finite Element Methods*, New York: CRC Press (2010).

39. Liu, G.R., Dai, K.Y., and Nguyen-Thoi, T. "A smoothed finite element for mechanics problems", *Computer and Mechanics*, **39**, pp. 859-877 (2007).

40. Liu, G.R., Nguyen-Thoi, T., Nguyen-Xuan, H., and Lam, K.Y. "A node based smoothed finite element method (NS-FEM) for upper bound solution to solid mechanics problems", *Computer and Structures*, **87**, pp. 14-26 (2009).

41. Nguyen-Thoi, T., Liu, G.R., Lam, K.Y., and Zhang, G.Y. "A face-based smoothed finite element method (FS-FEM) for 3D linear and nonlinear solid mechanics problems using 4-node tetrahedral elements", *International Journal for Numerical Methods in Engineering*, **78**, pp. 324-353 (2009).

42. Liu, G.R., Nguyen-Thoi, T., and Lam, K.Y. "An edge-based smoothed finite element method (ES-FEM) for static, free and forced vibration analyses of solids", *Journal of Sound and Vibration*, **320**, pp. 1100-1130 (2009).

43. Liu, G.R., Nguyen-Thoi, T., Dai, K.Y., and Lam, K.Y. "Theoretical aspects of the smoothed finite element method (SFEM)", *International Journal for Numerical Methods in Engineering*, **71**, pp. 902-930 (2007).

44. Liu, G.R., Nguyen-Xuan, H., and Nguyen-Thoi, T. "A theoretical study of S-FEM models: properties, accuracy and convergence rates", *International Journal for Numerical Methods in Engineering*, **84**, pp. 1222-1256 (2010).

45. Nguyen-Xuan, H., Rabczuk, T., Nguyen-Thoi, T., Tran, T.N., and Nguyen-Thanh, N. "Computation of limit and shakedown loads using a node-based smoothed finite element method", *International Journal for Numerical Methods in Engineering*, **90**, pp. 287-310 (2012).

46. Le, C.V., Nguyen-Xuan, H., Askes, H., Bordas, S., Rabczuk, T., and Nguyen-Vinh, H. "A cell-based smoothed finite element method for kinematic limit analysis", *International Journal for Numerical Methods in Engineering*, **83**, pp. 1651-1674 (2010).

47. Nguyen-Xuan, H., and Liu, G.R. "An edge-based finite element method (ES-FEM) with adaptive scaled-bubble functions for plane strain limit analysis", *Comput Methods Appl. Mech. Eng.*, **285**, pp. 877-905 (2015).

48. Nguyen-Xuan, H. and Rabczuk, T. "Adaptive selective ES-FEM limit analysis of cracked plane-strain structures", *Frontiers of Structural and Civil Engineering*, **9**, pp. 478-490 (2015).

49. Nguyen-Xuan, H., Wu, C.T., and Liu, G.R. "An adaptive selective ES-FEM for plastic collapse analysis", *European Journal of Mechanics A/Solid*, **58**, pp. 278-290 (2016).

50. Wu, S.C., Liu, G.R., Zhang, H.O., Xu, X., and Li, Z.R. "A node-based smoothed point interpolation method (NS-PIM) for three-dimensional heat transfer problems", *International Journal of Thermal Sciences*, **48**, pp. 1367-1376 (2009).

51. Cui, X.Y., Li, Z.C., Feng, H., and Feng, S.Z. "Steady and transient heat transfer analysis using a stable node-based smoothed finite element method", *International Journal of Thermal Sciences*, **110**, pp. 12-25 (2016).

52. Liu, G.R., Chen, L., Nguyen-Thoi, T., Zeng, K.Y., and Zhang, G.Y. "A novel singular node-based smoothed finite element method (NS-FEM) for upper bound solutions of fracture problems", *International Journal for Numerical Methods in Engineering*, **83**, pp. 1466-1497 (2010).

53. Wang, G., Cui, X.Y., Liang, Z.M., and Li, G.Y. "A coupled smoothed finite element method (S-FEM) for structural-acoustic analysis of shells", *Engineering Analysis with Boundary Elements*, **61,** pp. 207-217 (2015).

54. Wang, G., Cui, X.Y., Feng, H., and Li, G.Y. "A stable node-based smoothed finite element method for acoustic problems", *Computer Methods Applied Mechanics and Engineering*, **297**, pp. 348-370 (2015).

55. Cui, X.Y., Wang, G., and Li, G.Y. "A nodal integration axisymmetric thin shell model using linear interpolation", *Applied Mathematical Modelling*, **40**, pp. 2720-2742 (2016).

56. Feng, H., Cui, X.Y., and Li, G.Y. "A stable nodal integration method with strain gradient for static and dynamic analysis of solid mechanics", *Engineering Analysis with Boundary Elements*, **62**, pp. 78-92 (2016).

57. Wang, G., Cui, X.Y., and Li, G.Y. "A rotation-free shell formulation using nodal integration for static and dynamic analyses of structures", *International Journal for Numerical Methods in Engineering*, **105**, pp. 532-560 (2016).

58. Wang, G., Cui, X.Y., and Li, G.Y. "Temporal stabilization nodal integration method for static and dynamic analyses of Reissner-Mindlin plates", *Computers & Structures*, **152**, pp. 124-141 (2015).

59. Vo-Minh, T., Nguyen-Minh, T., Chau-Ngoc, A., and Nguyen-Chanh, H. "Stability of twin circular tunnels in cohesive-frictional soil using the node-based smoothed finite element method (NS-FEM)", *Journal of Vibroengineering*, **19**, pp. 520-538 (2017).

60. Mosek, The MOSEK optimization toolbox for MATLAB manual: http://www.mosek.com

61. Makrodimopoulos, A. and Martin, C.M. "Upper bound limit analysis using simplex strain elements and second-order cone programming", *International Journal for Numerical and Analytical Methods in Geomechanics*, **31**, pp. 835-865 (2006).

62. GiD 11.0.4, International Center for Numerical Methods in Engineering (CIMNE), Reference manual. http://www.cimne.com

63. Chen, W.F., *Limit Analysis and Soil Plasticity*, Elsevier, Amsterdam (1975).

## Biographies

**Thien Vo-Minh** received his BS and MS degrees in Civil Engineering from University of Technology, Ho Chi Minh City, Vietnam, in 1999 and 2002, respectively. He is currently a PhD Student at the Department of Geomechanics, Faculty of Civil Engineering, in the same University. He has authored one international journal paper related to the application of the upper bound limit analysis in geomechanical problems using the NS-FEM.

**An Chau-Ngoc** received his BS degree in Civil Engineering from University of Technology, Ho Chi Minh City, Vietnam in 1974, and his MS and PhD degrees in Geomecanique Materiaux from Institut National Polytechnique de Grenoble, France, in 1995, and 1999, respectively. He is currently an Associate Professor at the Department of Geomechanics, Faculty of Civil Engineering at the University of Technology, Ho Chi Minh City, Vietnam.

**Tam Nguyen-Minh** received his BS and MS degrees in Civil Engineering from Ho Chi Minh City University of Technology, Ho Chi Minh City, Vietnam in 1997 and 2001, respectively. He received his PhD from National University of Pukyong, Pusan City, Korea in 2006, and is currently an Associate Professor at the Geotechnical Department, Dean of Faculty of Civil Engineering at the Ho Chi Minh city University of Technology, Ho Chi Minh City, Vietnam.

**Hoang Nguyen-Chanh** received his BS and MS degrees in Civil Engineering from University of Technology, Ho Chi Minh City, Vietnam in 2010 and 2012, respectively. He is currently a PhD student at the Department of Geotechnics, Imperial College, London, UK.